An Eight-Port Circularly Polarized Wideband MIMO Antenna Based on a Metamaterial-Inspired Element for 5G mmWave Applications

Asif Khan, Yejun He, *Senior Member, IEEE*, and Zhi Ning Chen, *Fellow, IEEE*

***Abstract*—This letter presents a low-profile, single-layer wideband metamaterial-inspired circularly polarized (CP) multiple-input–multiple-output (MIMO) antenna array. An 8 × 8 antenna array is manufactured on the Rogers RT/Duroid 5880 substrate with a partial ground plane. The dimensions of the proposed MIMO antenna array are 0.285λ × 0.11λ × 0.001λ at 28 GHz, where λ is the free-space wavelength. The isolation, gain, and higher axial bandwidth ratio are significantly improved by the introduction of a metamaterial-inspired element. As a result, the proposed circularly polarized MIMO antenna has an impedance bandwidth of 18 GHz, a mutual coupling of no more than −20 dB, an axial ratio bandwidth (ARBW) of 13 GHz, and a peak gain of 20.5 dBi. Significantly, the designated mmWave band (25–29.5 GHz) for 5G communication is covered by the operating bandwidth of the antenna. MIMO parameters are also discussed in terms of cross-correlation, diversity gain, and mean effective gain to further investigate the performance of the MIMO antenna. Therefore, the suggested antenna array is a good candidate for 5G new radio (NR) smart devices and sensors.**

***Index Terms*—Circular polarization, cross-correlation, isolation, metamaterial, multiple-input–multiple-output.**

I. Introduction

THE multiple-input–multiple-output (MIMO) technologies can improve channel capacity without using more spectrum [1]. The isolation between array elements has a significant impact on how well MIMO systems work. The channel capacity, radiation efficiency, and envelope correlation coefficient (ECC) all suffer from inadequate isolation [2]. Additionally, in an N-by-N MIMO system, the channel capacity is extensively improved with increasing order [3], i.e., the system capacity may be increased by adding additional antenna components. However, the proximity of the several antenna components causes reduced isolation and low gain due to the limited size. Therefore, effective mutual coupling and low gain in millimeter-wave microstrip antennas are the main issues that researchers must deal with.

Several methods, such as polarization diversity [4], etched slots, self-isolation [5], and a parasitic element [6] were previously used to reduce mutual coupling. The current cancellation model is used for mutual decoupling [7]. However, the main disadvantages of these designs are high profiles, low gain, and narrow bandwidth.

Recently, a metamaterial structure has been used to improve the antenna's gain from 6 to 10 dBi [8]. To increase the antenna's gain, a hybrid approach of microstrip antenna array [9] together with the parasitic components [10] is used. Most of these procedures are often used for the single-element system.

Many 5G mmWave antennas (26/28 GHz band) are linearly polarized (LP). It can be observed in [11] and [12] that the circularly polarized (CP) MIMO antennas at the approved 5G frequency bands were designed, but they have narrow bandwidth and complex arrangement.

In this letter, we design a low-profile, wideband circularly polarized eight-port MIMO antenna array for mmWave applications. The ground cuts help to obtain a wide bandwidth while a metamaterial-inspired unit cell is used for isolation enhancement ≤ -20 dB. Additionally, the ground cuts also help to enhance gain and improve the axial ratio. According to the authors' best knowledge, it is the first paper for us to use the metasurface to improve three main parameters (isolation, gain, and circular polarization) of an octa-element MIMO antenna array on a single-layer substrate.

II. Antenna Element and Metamaterial Unit Cell Design and Analysis

A. Antenna Element Design

A schematic view of the single antenna is shown in Fig. 1(a). A tiny striped patch is first introduced; however, it shows no resonance response in mmWave band. In addition, an L-shaped stub is added from the top to the right side of the strip, and as a result of this iterative structure a dual-band antenna is obtained. Finally, another L-shaped stub is added to the left side of the strip, resulting in a wideband bandwidth from 22 to 40 GHz as seen in Fig. 1(b). The single antenna is further modified to an eight-port MIMO array and designed on a RO5880 substrate with 0.254 mm of thickness.

Manuscript received 2 January 2023; revised 17 February 2023; accepted 25 February 2023. Date of publication 3 March 2023; date of current version 7 July 2023. This work was supported in part by the National Natural Science Foundation of China under Grant 62071306; and in part by the Shenzhen Science and Technology Program under Grant JCYJ20200109113601723, Grant JSGG20210420091805014, and Grant JSGG20210802154203011. *(Corresponding author: Yejun He.)*

Asif Khan and Yejun He are with the State Key Laboratory of Radio Frequency Heterogeneous Integration, College of Electronics and Information Engineering, Shenzhen University, Shenzhen 518060, China (e-mail: asifm20019@gmail.com; heyejun@126.com).

Zhi Ning Chen is with the Department of Electrical and Computer Engineering, National University of Singapore, Singapore 119077 (e-mail: eleczn@nus.edu.sg).

Digital Object Identifier 10.1109/LAWP.2023.3251740

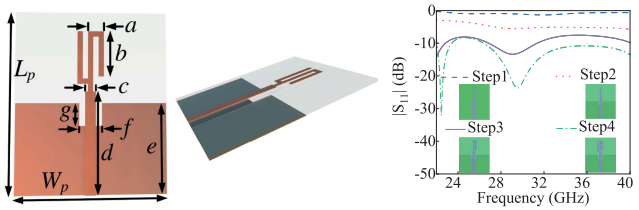

Fig. 1. (a) Designed single antenna front and side view. (b) $|S_{11}|$ of all four different cases.

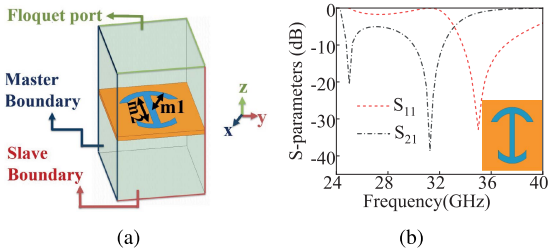

Fig. 2. (a) Unit cell's boundary conditions and excitation of Floquet port to determine the scattering characteristics. (b) S-parameters of the proposed unit cell.

B. Proposed Metamaterial-Inspired Element Design and Simulation

A unit cell size of 5×6 mm^2 is positioned on a 0.254 mm thick Rogers (5880) substrate. The given metamaterial-inspired element consists of two different arcs of the same ellipse and connected by a strip, resulting in an I-shaped unit cell, as shown in Fig. 2(a). On the x-axis and y-axis, master and slave boundary conditions are designed, while on the z-axis, the two ports are excited, respectively. Fig. 2(b) reveals the S-parameters of the proposed unit cell. It can be shown that the metasurface's unit cell resonates at 35 GHz and achieves a bandwidth of 5.5 GHz (33.5–39 GHz).

III. Evaluation of Eight-Element MIMO Antenna Array Band Optimized Results Comparison

The updated octa-element MIMO array is depicted in Fig. 3(a). The elements of the proposed MIMO antenna are placed on a Rogers (5880) substrate with a thickness of 0.254 mm. The return loss and insertion loss are displayed in Fig. 4(a) and (b), respectively. It provides a wide bandwidth of 18 GHz (22–40 GHz), whereas $|S_{11}| \leq -10$ dB, but the antenna's elements are highly mutually coupled ($|S_{21}| \geq -20$ dB), which degrades the performance of the MIMO antenna array. The optimized parameters of the designed antenna and unit cell are given in Table I.

A. Mutual Coupling Reduction

To decrease the mutual coupling, 9×2 I-shaped metamaterial-inspired unit cells are placed on the same substrate along with the antenna's elements in a periodic order. In this case, the reflection coefficients remain almost the same as both cases

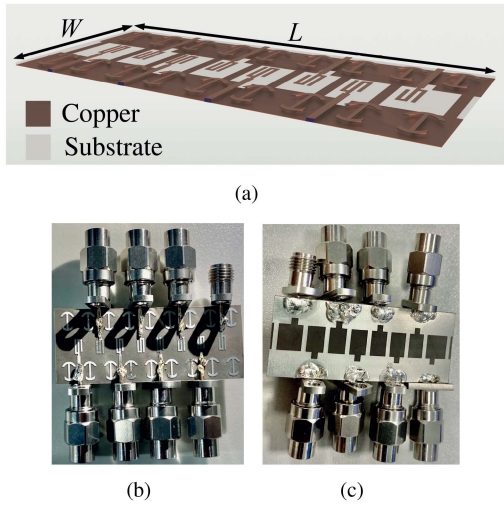

Fig. 3. (a) Geometry of the circular polarized 8-port MIMO antenna array along with metasurface and ground cut. (b) Fabricated front view. (c) Fabricated back view of the antenna array.

TABLE I
Optimized Parameters of the Designed Antenna and Unit Cell

Para.	Value (mm)	Para.	Value (mm)	Para.	Value (mm)
L_p	12	L	45.6	W_p	10
W	18	a	1	b	3
c	0.7	d	6.75	e	6
f	1.5	g	1.5	$m1$	2.3
$m2$	3.5				

(without and with metamaterial-inspired element), whereas mutual coupling ($|S_{21}|$, $|S_{76}|$, $|S_{28}|$, $|S_{35}|$, $|S_{81}|$, and $|S_{34}|$) is reduced by about 15 dB in overall bandwidth, which shows a significant improvement in isolation. The main reason of this improvement is that when we excite port-1 and terminate others, this 9×2 array of metamaterial-inspired elements scatters the transmitted current in other directions or absorbs (a little bit) or reflects it to port-1 rather than passing to other ports. The simulated and measured S-parameters of the given MIMO antenna are compared as shown in Fig. 4(d), (e), (f), and (g), respectively. It can be observed that the measured bandwidth ranges from 22 to 40 GHz ($|S_{11}| \leq -10$ dB), and the measured mutual coupling ($|S_{21}|$, $|S_{32}|$, and so on) is less than -20 dB, respectively. There is little difference between the simulated and measured results due to apparatus losses during measurement.

B. Mechanism of Gain Enhancement

The peak gain of the given MIMO antenna with and without metasurface is displayed in Fig. 5(a). The peak gain of the MIMO antenna without metamaterial-inspired element is 4, 5, and 1 dBi at 24, 28, and 38 GHz, respectively, when different ports are excited. The addition of metasurface significantly improves the gain of the proposed MIMO operation as it provides an additional resonance, which increases the system gain. Thus, the projected MIMO antenna with a metasurface delivers a high peak gain of up to 20.5 dBi at 24 GHz, which was 4 dBi without metasurface, meanwhile, it also improves the gain from 5 to

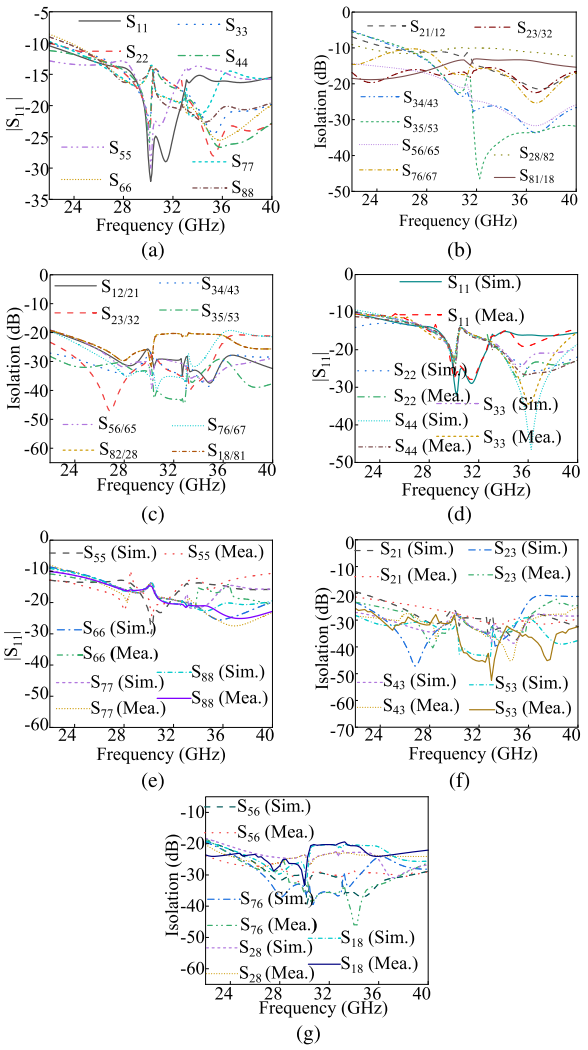

Fig. 4. (a) Simulated $|S_{11}|$ of the proposed MIMO antenna array. (b) Simulated mutual coupling without metasurface. (c) Simulated mutual coupling with metamaterial. (d) Comparison between simulated and measured $|S_{11}|$ (from element-1 to element-4). (e) Comparison between simulated and measured $|S_{11}|$ (from element-5 to element-8). (f) Comparison between simulated and measured mutual coupling (from element-1 to element-4). (g) Comparison between simulated and measured mutual coupling (from element-5 to element-8).

19 dBi and from 2 to 19.7 dBi at 28 and 38 GHz, respectively. The simulated and measured gains are well matched, as shown in Fig. 5(a).

C. Axial Ratio

Fig. 5(b) presents the simulated AR of the proposed MIMO antenna with and without metasurface. The MIMO antenna without metasurface has an ARBW of 4 GHz (24.5–26.5 GHz and 27–29 GHz) means that the antenna covers only one main operating frequency band of 28 GHz, but the ARBW is very narrow for a wideband antenna that has been operated in this article. This proposed MIMO antenna has a broad 3-dB AR bandwidth with multiple minimum AR points ranging from 22 to 26 GHz, 27 to 30 GHz, and 34 to 40 GHz after metamaterial integration. The combined effect of the alternative horizontally

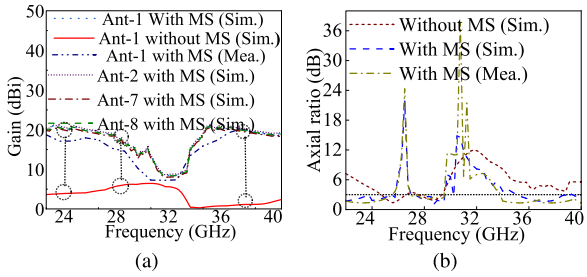

Fig. 5. (a) Simulated and measured gain with/without MS (metasurface). (b) Simulated and measured axial ratio with/without MS (metasurface).

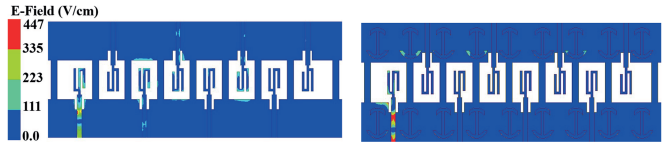

Fig. 6. Comparison of the surface current distribution on the radiated patch at 28 GHz (a) without and (b) with metamaterial.

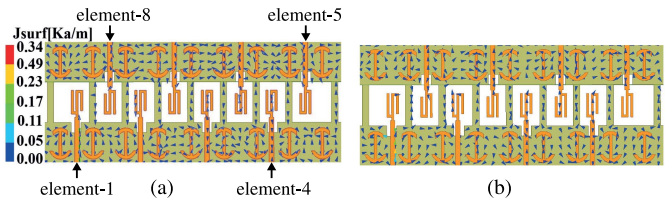

Fig. 7. Dispersion of current vectors on the radiated patch at different time phases of (c) 0° and (d) 90° at 28 GHz.

linearly polarized (HLP) and vertically linearly polarized (VLP) generation results in a circularly polarized wave when HLP and VLP waves for distinct angles (0° and 90°) are traveled toward the metasurface. The simulated and measured axial ratios accord well, as seen in Fig. 5(b).

D. Surface Current Distribution and Radiation Pattern

To further clarify how the metamaterial-inspired element contributes to isolation enhancement, the surface current distribution has been examined at 28 GHz. As shown in Fig. 6(a), when patch-1 is excited while the other ports are terminating, a flow of current to other ports is noticed means that the antennas are highly coupled. On the other hand, after the insertion of the metasurface, there is no flow of current appearing among the MIMO antenna's elements since the metasurface prevents the current from flowing to other ports, as shown in Fig. 6(b).

The surface current vector of the MIMO array at two-time phases (0° and 90°) is depicted in Fig. 7. This will help us further investigate the principle of the generation of circular polarization. According to Fig. 7(a) and (b), the arrows circulating around the patch-1 (when patch-1 is excited and the other ports are terminating in this case) in a clockwise direction means that it works as an LHCP device at (0° and 90°) at 28 GHz.

The proposed circularly polarized MIMO antenna without MS offers a consistent bidirectional radiation pattern with side lobe

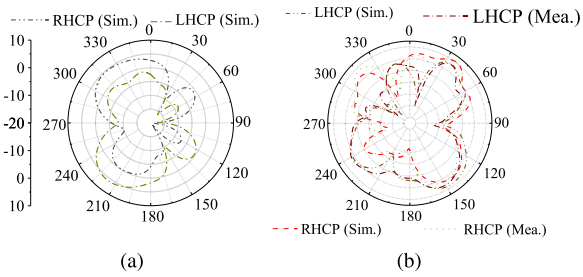

Fig. 8. Radiation patterns (LHCP and RHCP) of the given MIMO antenna array at 28 GHz (a) without and (b) with metamaterial-inspired element.

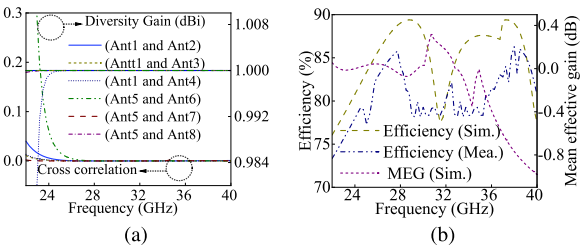

Fig. 9. (a) Cross-correlation and diversity gain of the eight-port CP MIMO antenna. (b) Radiation efficiency and mean effective gain.

values at 28 GHz. After inserting the metasurface, the radiation pattern has been disturbed a little bit by increasing the main lobe and back-lobe levels as shown in Fig. 8(a) and (b).

IV. MIMO Performances

To understand the characteristics of the MIMO antenna, it is essential to assess its diversity characteristics in terms of cross-correlation (CC), diversity gain (DG), and mean effective gain (MEG). A minimum signal correlation between the antenna's elements, which can be analyzed using CC, is important for a practical MIMO antenna. It can be calculated as

$$\rho_{porti,portj} = \frac{\frac{1}{2Z_0}\int\int_{\Omega} X_{porti}.X^*_{portj}d\Omega}{\sqrt{Y_{rad,porti}}\sqrt{Y_{rad,portj}}} \tag{1}$$

where Ω is the solid angle, while X_{porti} and X_{portj} are the antenna's far-fields when $porti$ and $portj$ are excited, respectively. In Fig. 9(a), the simulated CC for the working band is $\leq$0.005, indicating a low correlation between any two antennas.

In general, the value of the diversity gain (DG) for a MIMO antenna lies between 0 and 1 and can be expressed by

$$\text{DG} = \frac{mt(A^2)}{\|A\|_F} \tag{2}$$

where $\|A\|_F$ denotes the Frobenius norm of matrix A and $\|A\|_F = \sqrt{\sum_{i=l}^{m}\sum_{j=l}^{n}|a_{ij}|^2}$ for $A \in \mathbb{R}^{m\times n}$. mt represents the matrix trace of matrix A^2. Fig. 9(a) also presents the plots of diversity gain among all the MIMO antenna's elements, which are approximately 0.9999 dBi.

The MEG analyzes the gain between antenna elements while taking into account real propagation conditions. MEG for port i is given by

$$\text{MEG}_{porti} = 0.5\eta_{i,rad} = 0.5\left[1 - \sum_{j=1}^{K}|S_{ij}|^2\right] \tag{3}$$

where K and η_i indicate the number of antennas and radiation efficiency, respectively. The MIMO antenna with better performance should have a value of MEG less than -3 dB [6], while the value for the MEG of the proposed MIMO antenna array is less than 1 dB, as shown in Fig. 9(b).

As far as the radiation efficiency of the suggested MIMO antenna array within the operation band is concerned, the achieved radiation efficiency is more than 75%, as shown in Fig. 9(b).

TABLE II
Comparison to Other Multiport mmWave Mimo Antennas

	[4]	[7]	[11]	[13]	This work
Number of ports	2	4	4	4	8
Bandwidth ($\|S_{11}\|\leq$-10 dB)	26.9-30.7	25.5-26.5	18.62-20.40, 27.15-30.35	26.4-32.7	22-40
Spacing elements (λ)	0.04	0.48	1.27	1	0.02
Isolation S_{21} (dB)	-37	-35	-28	-35	-20
Polarization	CP	NA	CP	NA	CP
Size (Length, width, thickness) (mm)	20 27 2.5	23 6.5 0.508	NA	30 15 0.254	45.6 18 0.254
Peak gain (dBi)	11.9	NA	5.75,4.77	5.42	20.5

Table II shows the comparative study of the proposed work in the manuscript with other MIMO antenna arrays for mmWave applications. None of the works previously reported in the literature obtained a wide bandwidth of more than 5 GHz except [13], where the achieved bandwidth was 6.3 GHz, but the spacing between the antennas elements is relatively larger than the proposed one. Considering 5G communication service at 28 GHz band, the peak gain values are not above 10 dBi for most of the designs except [4], which is 11.9 dBi in Table II. In contrast, the given MIMO antenna array design provides a wide-band coverage of 18 GHz while having a mutual coupling level below -20.73 dB, and a lower peak gain value is also above 8 dBi in the entire operating band.

V. Conclusion

In this letter, a very compact CP octaelement MIMO antenna with multiple unique metamaterial-inspired unit cells is presented. The enhanced mutual coupling reduction and circular polarization are achieved by employing the metasurface to tickle the current fields and generate the current distribution on the MIMO antenna's elements. When the CP antennas are aligned with an edge-to-edge distance of 0.02λ, the designed CP MIMO antenna array has an impedance bandwidth of 18 GHz, mutual coupling less than -20 dB, AR bandwidth of 13 GHz, and peak gain of 20.5 dBi. The results of these parameters demonstrate that the suggested antenna performs very well.

REFERENCES

[1] R. He, B. Ai, G. L. Stuber, G. Wang, and Z. Zhong, "Geometrical-based modeling for millimeter-wave MIMO mobile-to-mobile channels," *IEEE Trans. Veh. Technol.*, vol. 67, no. 4, pp. 2848–2863, Apr. 2018.

[2] R. Janaswamy, "Effect of element mutual coupling on the capacity of fixed length linear arrays," *IEEE Antennas Wireless Propag. Lett.*, vol. 1, pp. 157–160, 2002.

[3] M. Golmohamadi and J. Frolik, "A geometric scattering model for circularly polarized indoor channels," *IEEE Trans. Antennas Propag.*, vol. 68, pp. 2290–2296, Mar. 2020.

[4] U. Ullah, M. Al-Hasan, S. Koziel, and I. B. Mabrouk, "Series-slot-fed circularly polarized multiple-input–multiple-output antenna array enabling circular polarization diversity for 5G 28 GHz indoor applications," *IEEE Trans. Antennas Propag.*, vol. 69, no. 9, pp. 5607–5616, Sep. 2021.

[5] S. Roy, S. Ghosh, and U. Chakarborty, "Compact dual wide-band four/eight elements MIMO antenna for WLAN applications," *Int. J. RF Microw. Comput. Aided Eng.*, vol. 29, no. 7, pp. 1–15, 2019.

[6] A. Khan, Y. He, Z. He, and Z. N. Chen, "A compact quadruple-band circular polarized MIMO antenna with low mutual coupling," *IEEE Trans. Circuits Syst. II: Exp. Briefs*, early access, 2022.

[7] W. Song, X.-W. Zhu, L. Wang, and W. Hong, "Simple structure E-plane decoupled millimeter wave antenna based on current cancellation model," *IEEE Trans. Antennas Propag.*, vol. 70, no. 10, pp. 9871–9876, Oct. 2022.

[8] A. Dadgarpour, A. A. Kishk, and T. A. Denidni, "Dual band high-gain antenna with beam switching capability," *Microw., Antennas Propag.*, vol. 11, no. 15, pp. 2155–2161, 2017.

[9] M. Khalily, R. Tafazolli, P. Xiao, and A. A. Kishk, "Broadband mm-wave microstrip array antenna with improved radiation characteristics for different 5G applications," *IEEE Trans. Antennas Propag.*, vol. 66, no. 9, pp. 4641–4647, Sep. 2018.

[10] K. Ding, C. Gao, T. Yu, D. Qu, and B. Zhang, "Gain-improved broadband circularly polarized antenna array with parasitic patches," *IEEE Antennas Wireless Propag. Lett.*, vol. 16, pp. 1468–1471, 2017.

[11] M. A. Sofi, K. Saurav, and S. K. Koul, "Four-port orthogonal circularly polarized dual-band MIMO antenna with polarization and spatial diversity using a dual-band linear-to-circular polarization converter," *IEEE Trans. Antennas Propag.*, vol. 70, no. 9, pp. 8554–8559, Sep. 2022.

[12] K. R. Mahmoud and A. M. Montaser, "Synthesis of multi-polarised upside conical frustum array antenna for 5G mm-wave base station at 28/38 GHz," *IET Microw., Antennas Propag.*, vol. 12, no. 9, pp. 1559–1569, 2018.

[13] N. Hussain, W. A. Awan, W. Ali, S. I. Naqvi, A. Zaidi, and T. T. Le, "Compact wideband patch antenna and its MIMO configuration for 28 GHz applications," *AEU-Int. J. Electron. Commun.*, vol. 132, Apr. 2021, Art. no. 153612.